01 Dec 2021

Temperature And Strain Sensing With Hybrid Interferometer

Lashari Ghulam Abbas

Zhou Ai

Farhan Mumtaz
Missouri University of Science and Technology, mfmawan@mst.edu

Atta Muhammad

et. al. For a complete list of authors, see https://scholarsmine.mst.edu/ele_comeng_facwork/5062

Recommended Citation

Temperature and Strain Sensing With Hybrid Interferometer

Lashari Ghulam Abbas[ID], Zhou Ai[ID], Farhan Mumtaz[ID], Atta Muhammad, Yutang Dai[ID], and Rashda Parveen[ID]

Abstract—A hybrid interferometer for simultaneous measurement of strain and temperature is proposed and investigated experimentally. This hybrid design is composed of Fabry-Perot interferometer (FPI) and Michelson Interferometer (MI) cascaded with each other. It is developed by fusion splicing a single mode fiber (SMF), a multimode fiber (MMF), a dual side hole fiber (DSHF), a hollow core fiber (HCF) and a tapered-SMF. The tapered SMF was inserted into the HCF to form a reflection mirror for the FPI. The maximum temperature and strain sensitivity of the hybrid interferometer achieved through experiments is 11.6 pm/$^\circ$C and 6.8 pm/$\mu\varepsilon$, respectively. The different sensitivities of FPI and MI to temperature and strain enable us to achieve simultaneous measurement. The proposed hybrid interferometer sensor has many attractive features such as, novel design, low cost, easy fabrication, compact size, and good sensitivity. Therefore, the proposed hybrid sensor could be widely deployed in plenty of applications, for instance, structural health monitoring, civil engineering, food manufacturing, chemical and medical fields.

Index Terms— Hybrid interferometer, strain sensor, dual side hole fiber.
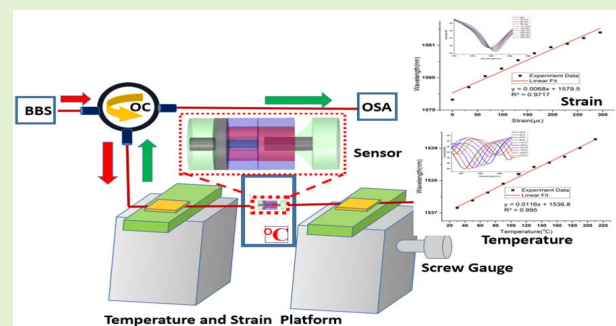
I. INTRODUCTION

OPTICAL fiber sensors are extensively deployed in several disciplines such as, biomedical [1], food processing [2], chemical [3], smart textiles [4], civil [5], marine structures monitoring [6], and aerospace [7], due to their resistance to electromagnetic interference, low cost, fast response, compact size, light weight, and high stability in harsh environments.

Lashari Ghulam Abbas is with the National Engineering Laboratory for Fiber Optic Sensing Technology, Wuhan University of Technology, Wuhan 430070, China, and also with the Electrical Engineering Department, Sukkur IBA University, Sukkur 65200, Pakistan (e-mail: ghulamscut@gmail.com).

Zhou Ai and Yutang Dai are with the National Engineering Laboratory for Fiber Optic Sensing Technology, Wuhan University of Technology, Wuhan 430070, China (e-mail: zhouaipost@hotmail.com; daiyt6688@whut.edu.cn).

Farhan Mumtaz is with the National Engineering Laboratory for Fiber Optic Sensing Technology, Wuhan University of Technology, Wuhan 430070, China, and also with the Communications Laboratory, Department of Electronics, Quaid-i-Azam University, Islamabad 45320, Pakistan (e-mail: mfmawan@whut.edu.cn).

Atta Muhammad is with the Telecommunication Engineering Department, Quaid-e-Awam University of Engineering, Science and Technology, Nawabshah 67480, Pakistan (e-mail: attapanhyar@quest.edu.pk).

Rashda Parveen is with the Communications Laboratory, Department of Electronics, Quaid-i-Azam University, Islamabad 45320, Pakistan (e-mail: rashda@ele.qau.edu.pk).

Digital Object Identifier 10.1109/JSEN.2021.3120798

Recently, many types of fiber optic sensors are developed using several methods for multiparameter sensing applications for example, long-period fiber grating (LPFG) [8]–[10], fiber Brag grating (FBG) [11]–[15], using CO_2 and femtosecond laser. However, sensors based on gratings are fundamentally susceptible to cross-sensitivity issues and require most expensive equipment for manufacturing. Various interferometers have been used for measuring more than one physical parameters such as, Optical fiber modal interferometers [16]–[18], Michelson interferometers (MI) [19]–[21], hybrid interferometers (MZI, MI and FPI) [22]–[25]. Mach–Zehnder interferometers (MZI) [26]–[29], and Fabry–Perot interferometers (FPI) [30]–[33]. Measurement of one physical parameter in the presence of another using fiber optics sensors is a challenging task such as, measuring strain in the presence of temperature can introduce some cross-sensitivity issues. To diminish the effect of cross-sensitivity, several configurations have been developed to measure two or more than two physical parameters, simultaneously. Frazao et al, used a hybrid structure with FPI and MI interferometers for measurement of strain and temperature [34]. Hao et al, developed a hybrid structure, which consists of FPI and MI for measuring refractive index and temperature, simultaneously [31]. Zhou et al, developed a hybrid structure consists of cascaded fabry-perot interferometers for measuring temperature and strain, simultaneously [23]. Zhu et al, developed a hybrid structure for measuring transverse load and temperature simultaneously [22]. Najari et al, developed a hybrid structure based on MZI for measuring strain and temperature simultaneously [29]. Ni et al, developed
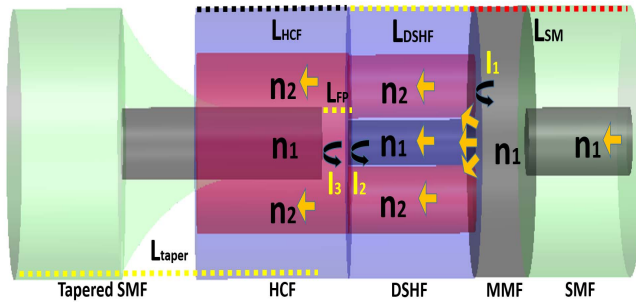
Fig. 1. Schematic diagram of the hybrid sensor.

Fig. 2. Fabrication stages of the hybrid sensor.

a hybrid structure based on MZI for measuring refractive index and temperature simultaneously [26]. Therefore, taking in view the requirements of the modern industry, it is necessary to design and manufacture a novel sensor for measuring temperature and strain, simultaneously. The novel sensor should be highly sensitive, compact, inexpensive, and easy to reproduce using simple steps. In this article, we have proposed a hybrid interferometer for measuring the temperature and strain, simultaneously. It is manufactured by cascading Fabry-Perot interferometer with Michelson interferometer. FPI is composed of air-cavity, which is sensitive to axial strain and insensitive to temperature, while the MI consists of silica cavity, which is sensitive to temperature and insensitive to axial strain. Therefore, such a hybrid interferometric structure is viable for simultaneous measurement of temperature and strain. The main features of the proposed hybrid interferometric sensor are its novel design, compact size, low cross-sensitivity, cost-effective manufacturing, good sensitivity and ability to measure dual parameters simultaneously. Therefore, the proposed sensor could be widely deployed in numerous fields of science and engineering.

The remaining part of this manuscript consists of the following sections. Part II defines the fabrication procedure and the working principle of the hybrid interferometer. In Part III, the results for strain and temperature are discussed in detail. Lastly, the Part IV concludes the whole work of the article.

II. FABRICATION PROCEDURE AND WORKING PRINCIPLE

Now-a-days, simultaneous measurement of more than one parameters is the widely researched aspect in optical fiber sensing. Many researchers used hybrid structures based on interferometers [23], FBG [13], and LPFG [8] for the measurement of multi-parameters. There is need of such type of sensors that might be useful in simultaneous measurement of two or more physical parameters. Simultaneous measurement of strain and temperature has applications in civil engineering, aerospace and many other related fields. Therefore, we designed and fabricated the proposed structure to meet the current industrial requirements.

The novel hybrid interferometer is schematically presented in Fig. 1. Its structure involves tapered-SMF, HCF, DSHF, MMF and SMF. The tapered-SMF with waist diameter of
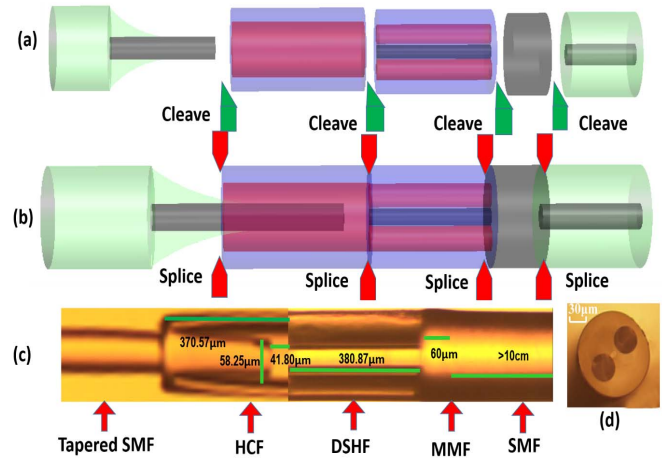
about 60 μm has been put into the HCF to form FPI cavity. The HCF has the core and the cladding diameter of 62 μm and 125 μm, respectively. The DSHF consists of a cladding, two side air holes, and an elliptical central silica core. The diameter of the cladding and each of the two air holes is 125 μm and 40 μm, respectively. The diameter of the central silica core at the major and the minor axis is 11.4 μm and 8.7 μm, respectively. MMF has the core and the cladding diameter of 8.2 μm and 125 μm, respectively. The diameter of the core and the cladding of the SMF is 8.2 μm and 125 μm, respectively.

Length of each fiber for sample S1 is displayed in Fig.2, and the taper waist, length of the HCF and DSHF for sample S1 and S2 are given in Table I. In order to get the accurate length, we made several samples with different lengths and the samples with better results were included in the manuscript. Fiber cleaver with the electronic microscope was used to cut each fiber close to the required length. After fusion splicing, we measured the length with 0.01μm accuracy using a software associated with the microscope (LT/UPR203i) as shown in Fig.2. The production procedure of the proposed sensor involves cleaving, fusion splicing and tapering techniques.

The production of the hybrid interferometer involves the following steps. Initially, the high precision cleaver was used to cleave all the fibers including SMF, MMF, DSHF and HCF, as shown in Fig. 2(a). Secondly, a piece of SMF was subjected to a tapering machine (Kaipule Co. Ltd. AFBT-8000MX-H) in order to obtain the one end taper of SMF using a hydrogen-oxygen flame. The software associated with the tapering machine was utilized to control the amount of hydrogen-oxygen flame required for the SMF tapering and the pulling speed of the stepper motors. SMF fiber was fixed over the tapering platform, which is operated by two stepper motors from each side. The center of the SMF was heated by the flame of hydrogen-oxygen gas. In the meantime, the SMF was pulled by two stepper motors at fixed speed as the pulling speed contributes a lot to get the different diameters of the fiber. For verification of the tapered-SMF diameter, it was observed under the microscope. The tapering process was continued

until the taper waist diameter was reduced to ∼60 μm. The diameter of the fiber on the outer edge was kept thicker to get maximum reflection.

Thirdly, the cleaved SMF, MMF, DSHF and the HCF were spliced together in a cascaded manner using the polarization maintaining fusion splicer (FSM-40PM). So as to fusion splice all fibers firmly and to avoid the collapsing of the HCF, DSHF, and tapered-SMF, different values of the discharge current and discharge time were carefully chosen. Table II, describes the splicing parameters for the hybrid interferometer.

Fourthly, after cleaving the tapered SMF, it was inserted into the HCF to get the FPI cavity. The taper insertion process was carried out using the Fusion Splicing machine and the reflection spectrum was monitored using OSA in order to get the suitable length of the FPI cavity. The insertion of the tapered SMF into the HCF was stopped, when the required cavity length was achieved. Then, both fibers were fusion spliced using manual splicing program to obtain the proper sealed FPI cavity, as shown in Fig 2(b). The microscopic view of the proposed interferometer is presented in Fig 2(c). This image was captured with the microscope (LT/UPR203i), which has built-in camera known as the charged coupled device (CCD). The captured image can be easily transferred to PC for further analysis. It can be seen from the image that the fusion spliced connection is robust and offer better durability to the hybrid design. As a result, the design seems more firm and durable in comparison to the offset spliced structures [33]. The micrograph of the DSHF cross-section is presented in Fig 2(d).

The propagation of the optical beams in the newly designed hybrid interferometer is shown in Fig. 1. There are mainly three light beams I_1, I_2, and I_3 propagating in the hybrid structure. The incoming light beam entered into the MMF after passing through the SMF. This light beam was distributed into multiple light beams after entering into the MMF. One light signal I_1 returned back from the junction between the MMF and the air holes of the DSHF, but the remaining light successfully propagated through the silica and the air paths of the DSHF. Further, the beams passing through DSHF propagated through HCF but the beam I_2 transmitting through the silica core of the DSHF returned back from the interface between DSHF and HCF. Consequently, these two light signals I_1 and I_2 interfered with each other and formed the Michelson interferometer. Similarly, the beam I_3 returned back from the junction between the SMF (Taper) and the HCF, also mixed with the beam I_2. Thus, the interference of the two beams I_2, and I_3 formed the Fabry-Perot Interferometer. The light beams propagating through the two side air holes of the DSHF

were not discussed because, not only its energy is less than that passing through the silica part of the DSHF, but also its propagation loss is higher than that in the silica part. When the light beams I_1, I_2, and I_3 are mixed and the resultant interference signal becomes the superposition of the FPI and MI interference.

The light intensities of the MI (I_1, I_2) and FPI (I_2, I_3) can be written as

$$I_{MI} = I_1 + I_2 + 2\sqrt{I_1 . I_2} \cos(\theta_1) \qquad (1)$$

$$I_{FPI} = I_2 + I_3 + 2\sqrt{I_2 . I_3} \cos(\theta_2) \qquad (2)$$

where θ_1 and θ_2 represent the phase difference of Michelson and Fabry-Perot Interferometers, respectively. It can be defined as, $\theta_1 = 4\pi n_1 L_{DSHF}/\lambda_1$, and $\theta_2 = 4\pi n_2 L_{FP}/\lambda_2$, where L_{DSHF} represents the length of the silica cavity and the L_{FP} denotes the length of the air cavity, n_1 represents the refractive index of the silica core of the DSHF, core of the SMF and the core of the MMF. n_2 denotes the refractive index of the air core of the HCF and the side air holes of the DSHF, λ denotes the source wavelength. As the phase difference meets the following condition, the resonant dips will appear at the wavelength $\lambda_{MI} = 2n_1 L_{DSHF}/p$ and $\lambda_{FP} = 2n_1 L_{FP}/q$, where $p.q = 0,1,2\ldots$. The Free Spectral Range (FSR) for the MI and the FPI, can be expressed as, $FSR_{MI} = \lambda^2/2(n_1 L_{DSHF})$ and $FSR_{FP} = \lambda^2/2(n_2 L_{FP})$. The change in the length of HCF is directly proportional to the change in the length of FP cavity. Because the force is exerted at the junction between the HCF and the tapered SMF. Therefore, $\Delta L_{HCF} = \Delta L_{FP}$.

The longitudinal strain is applied on the total length L

$$L = L_{SM} + L_{DSHF} + L_{HCF} + L_{taper} \qquad (3)$$

where L_{SM}, L_{DSHF}, L_{HCF}, L_{taper}, are the lengths of SMF-MMF, DSHF, HCF, and tapered SMF, respectively. Therefore, the relationship of the applied strain is expressed as,

$$\varepsilon_{SM} E A_{SM} = \varepsilon_{DSHF} E A_{DSHF} = \varepsilon_{HCF} E A_{HCF}$$
$$= \varepsilon_{taper} E A_{taper} \qquad (4)$$

where E is the young modulus of the material, A_{SM}, A_{DSHF}, A_{HCF}, A_{taper} are the cross-sectional areas of the SMF-MMF, DSHF, HCF, and tapered SMF, respectively. ε_{SM}, ε_{DSHF}, ε_{HCF}, ε_{taper} are the longitudinal strain of the SMF-MMF, DSHF, HCF, and tapered SMF, respectively.

$$\varepsilon_{SM} = \frac{\Delta L_{SM}}{L_{SM}}, \quad \varepsilon_{DSHF} = \frac{\Delta L_{DSHF}}{L_{DSHF}}, \quad \varepsilon_{HCF} = \frac{\Delta L_{HCF}}{L_{HCF}},$$

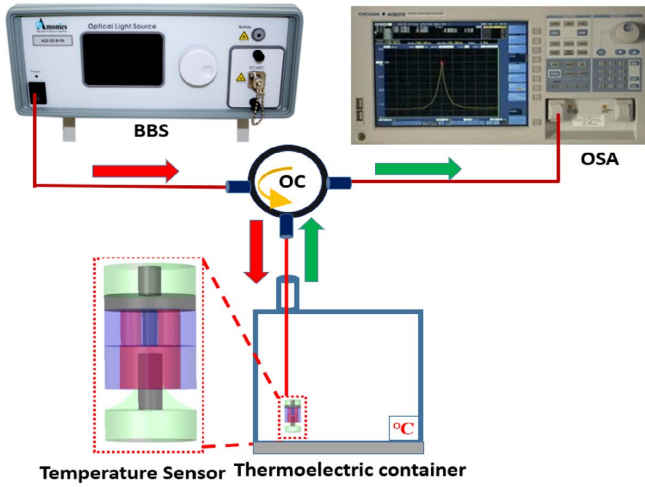$$\varepsilon_{taper} = \frac{\Delta L_{taper}}{L_{taper}} \qquad (5)$$

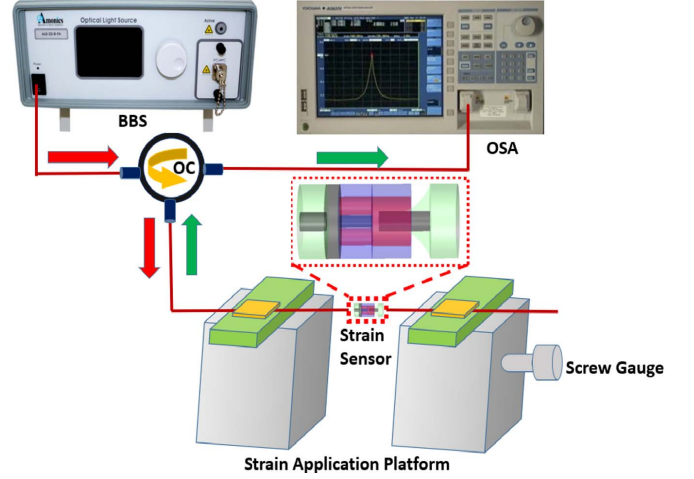Fig. 3. Temperature measurement setup for Hybrid sensor.

Fig. 4. Strain measurement setup for Hybrid sensor.

The total longitudinal strain is given by

$$\varepsilon_L = \frac{\Delta L_{SM} + \Delta L_{DSHF} + \Delta L_{HCF} + \Delta L_{taper}}{L_{SM} + L_{DSHF} + L_{HCF} + L_{taper}} \qquad (6)$$

Relationship between ε_L and ε_{DSHF} is given as,

$$\varepsilon_{DSHF}$$
$$= \frac{L_{SM} + L_{DSHF} + L_{HCF} + L_{taper}}{L_{SM}\frac{A_{DSHF}}{A_{SM}} + L_{DSHF} + L_{HCF}\frac{A_{DSHF}}{A_{HCF}} + L_{taper}\frac{A_{HCF}}{A_{taper}}}.\varepsilon_L \qquad (7)$$

Similarly, the relationship between ε_L and ε_{HCF} is given as,

$$\varepsilon_{HCF}$$
$$= \frac{L_{SM} + L_{DSHF} + L_{HCF} + L_{taper}}{L_{SM}\frac{A_{HCF}}{A_{SM}} + L_{DSHF}\frac{A_{HCF}}{A_{DSHF}} + L_{HCF} + L_{taper}\frac{A_{HCF}}{A_{taper}}}.\varepsilon_L \qquad (8)$$

The relationship between change in wavelength due to axial strain for air cavity and silica cavity is given as,

$$S_{FP(\varepsilon)} = \Delta\lambda_{FP} = \lambda_{FP}\varepsilon_{HCF} \qquad (9)$$
$$S_{MI(\varepsilon)} = \Delta\lambda_{MI} = \lambda_{MI}\varepsilon_{DSHF} \qquad (10)$$

The temperature sensitivities of the air cavity and the silica cavity is given as,

$$S_{FP(T)} = \Delta\lambda_{FP} = \lambda_{FP}(\frac{1}{n_2}.\frac{\Delta n_2}{T} + \frac{1}{L_{FP}}.\frac{\Delta L_{FP}}{T})\Delta T$$
$$= \lambda_{FP}(\alpha_{air} + \xi_{air})\Delta T \qquad (11)$$
$$S_{MI(T)} = \Delta\lambda_{MI} = \lambda_{MI}(\frac{1}{n_1}.\frac{\Delta n_1}{T} + \frac{1}{L_{DSHF}}.\frac{\Delta L_{DSHF}}{T})\Delta T$$
$$= \lambda_{MI}(\alpha_{si} + \xi_{si})\Delta T \qquad (12)$$

where $\xi_{si}\alpha_{si}$, α_{air},ξ_{air} represent the thermos-optic coefficient and thermal expansion coefficient of the silica and air, respectively.

III. EXPERIMENTAL RESULTS

The experimental apparatus used to measure temperature and strain is shown in Fig. 3. and Fig. 4., respectively. In the hybrid interferometer, the light was input through a broadband light source with an operating wavelength of 1500 nm. The reflected light signals were collected by an optical coupler. An Optical Spectrum Analyzer (OSA) with the wavelength resolution of 0.1 nm was used to monitor the reflection spectrum of the sensor.

Two samples of the hybrid interferometer with different lengths of FPI (air cavity) and MI (silica cavity) were manufactured and their temperature response was investigated through experiments. In order to achieve the unique FSR, the DSHF, and HCF lengths were set slightly different. We formulated $FSR_{MI} = \lambda^2/2(n_1 L_{DSHF})$ and $FSR_{FP} = \lambda^2/2(n_2 L_{FP})$ to calculate the FSR of the two interferometers and then these equations were used to obtain the proper lengths of the DSHF and HCF. Several samples of the proposed hybrid sensor were developed and the lengths of all the fibers were chosen different in order to reduce the fabrication errors and to obtain the optimized length of each fiber. Figure 5(a), (b), and (c), illustrate the reflection spectrum of the hybrid sensor, silica cavity (MI), and air cavity (FPI), respectively. The measured free spectral range (FSR) of the envelope of the proposed sensor is 30 nm, which corresponds well with the theoretical results.

In order to investigate the sensing characteristics of the hybrid interferometer, the experimental system illustrated in Fig. 3, was used. To observe the temperature response of the proposed hybrid sensor, it was put into a thermoelectric box with a resolution of 0.1 °C. The thermometer lead was also put in the thermoelectric box to record the temperature change. The wavelength shift versus temperature of the hybrid interferometer were obtained at temperature ranging 30 °C to 210°C with a step of 20°C, as shown in Fig. 6 and Fig. 7, respectively. It can be seen that the temperature sensitivities of both samples are similar for FPIs as well as for MIs in the hybrid structure. The temperature sensitivities of two samples of FPIs are 1.3 pm/°C and 1.4 pm/°C. The temperature
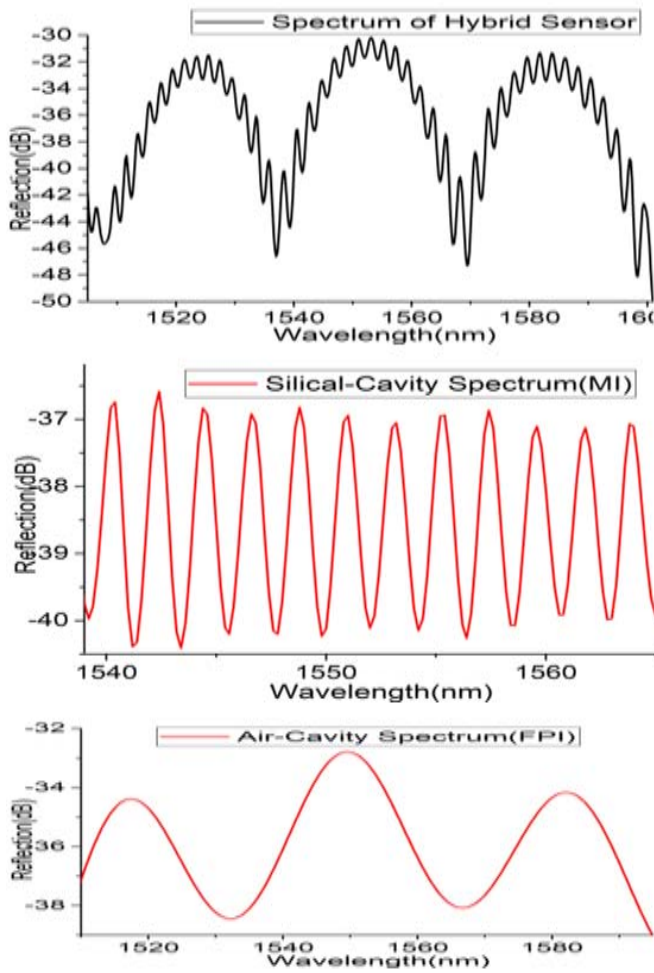
Fig. 5. Spectrum of the (a) Hybrid Interferometer (b) Silica Cavity (MI) (c) Air Cavity (FPI).
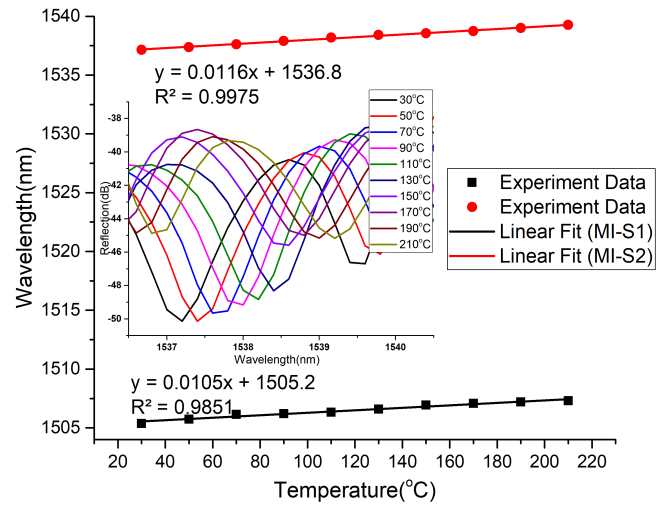

Fig. 6. Linear fitting curve and reflection spectra(inset) of Michelson Interferometer (S1 & S2) under different temperature values.
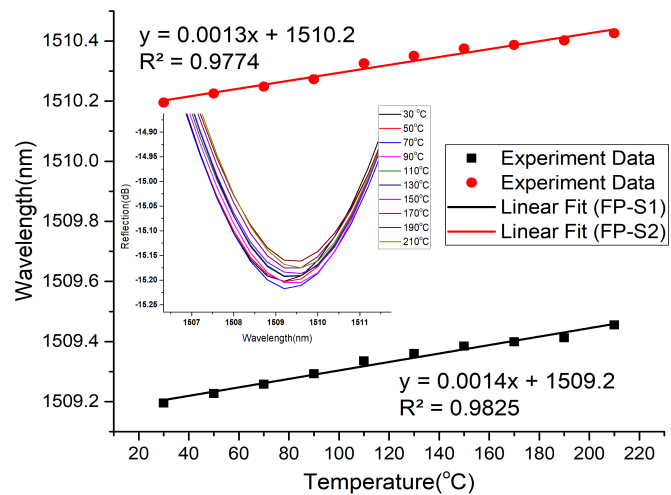

Fig. 7. Linear fitting curve and reflection spectra(inset) of Fabry-Perot Interferometer (S1 & S2) under different temperature values.

sensitivities of the two samples of MI are 10.5 pm/°C and 11.6 pm/°C, which approximate 8 times those of the FPIs, and are comparable to single silica cavity-based sensors.

The same two samples of the hybrid interferometer with different lengths of FPI (air cavity) and MI (silica cavity) were also used for strain sensing and their strain response was investigated through experiments. In order to achieve the unique FSR, the DSHF, and HCF lengths were set slightly different. We formulated $FSR_{MI} = \lambda^2/2(n_1 L_{DSHF})$ and $FSR_{FP} = \lambda^2/2(n_2 L_{FP})$ to calculate the FSR of the two interferometers and then these equations were used to obtain the proper lengths of the DSHF and HCF. Numerous samples of the proposed hybrid sensor were developed and the lengths of all the fibers were chosen different in order to reduce the fabrication errors and to obtain the optimized length of each fiber.

To analyze the strain effect on the proposed hybrid sensor, it was attached with strain application platform, which has fixed and movable parts. The rotatable part comprises a micrometer screw gauge, which was used to apply the longitudinal strain on the hybrid sensor with step of $\sim$33 pm/$\mu\varepsilon$. The output spectra of the hybrid interferometer were recorded

at applied strain ranging from 0 $\mu\varepsilon$ to 300 $\mu\varepsilon$ with a step of $\sim$33 $\mu\varepsilon$. The inset illustrates the structure of the proposed hybrid sensor developed for strain sensing. The wavelength shift versus strain of the MI and FPI were obtained at applied axial strain ranging from 0 $\mu\varepsilon$ to 300 $\mu\varepsilon$ with a step of 33 $\mu\varepsilon$, as shown in Fig. 8 and Fig. 9, respectively.

It shows that the strain sensitivities of both samples are similar for FPIs as well as MIs. The axial strain sensitivity of the two samples of MI is 1.1 pm/$\mu\varepsilon$ and 1.3 pm/$\mu\varepsilon$. Whereas, the axial strain sensitivity of the two samples of FPIs are 6.7 pm/$\mu\varepsilon$ and 6.8 pm/$\mu\varepsilon$, which are 6 times higher than the strain sensitivity of the MIs and single silica cavity-based sensors.

Experimental results ensure that the proposed hybrid interferometer, which is manufactured by cascading FPI with MI sensor can measure the temperature and strain, simultaneously. Because, FPI is composed of air-cavity, which is sensitive to axial strain and insensitive to temperature, whereas the MI
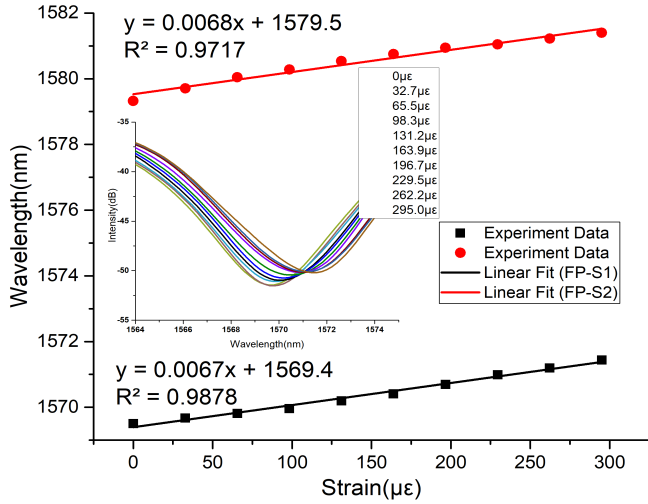
Fig. 8. Linear fitting curve and reflection spectra(inset) of Fabry-Perot Interferometer (S1 & S2) under different strain values.
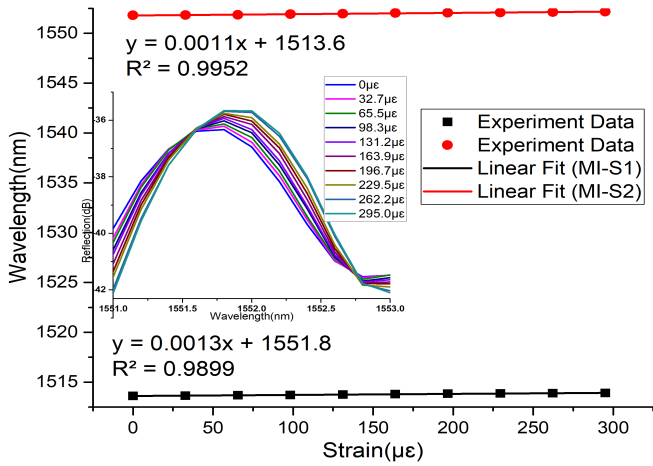

Fig. 9. Linear fitting curve and reflection spectra(inset) of Michelson Interferometer (S1 & S2) under different strain values.

consists of silica cavity, which is sensitive to temperature and insensitive to axial strain. Therefore, such a hybrid interfero-metric structure is applicable for measuring temperature and strain, simultaneously. The reflection spectrum of the hybrid interferometer shifts when subjected to temperature and strain. The two interferometers, FPI and MI have different responses to these physical parameters. The linear superposition of the resultant wavelength can be seen when two quantities are investigated, simultaneously. Therefore, the wavelength changes of the two interferometers due to temperature and strain can be mathematically described as

$$\Delta \lambda_i = k_{Ti} \Delta T + k_{\varepsilon i} \Delta \varepsilon; \quad i = FP, MI \quad (13)$$

The coefficient matrix based on the above equation can be written as

$$\begin{bmatrix} \Delta \lambda_{FP} \\ \Delta \lambda_{MI} \end{bmatrix} = \begin{bmatrix} K_{T,FP} & K_{\varepsilon,FP} \\ K_{T,MI} & K_{\varepsilon,MI} \end{bmatrix} \begin{bmatrix} \Delta \varepsilon \\ \Delta T \end{bmatrix} \quad (14)$$

where ΔT and $\Delta \varepsilon$ are the temperature and strain variations, respectively. $\Delta \lambda_{FP}$ and $\Delta \lambda_{MI}$ denote the change in the wave-

TABLE III
SENSITIVITY COMPARISON OF HYBRID INTERFEROMETER

Configuration	Strain(pm/με)	Temperature(pm/°C)	Reference
FMF + FBG	0.91	11.5	[35]
FMF + FBG	0.8778	9.9214	[36]
FPI + FBG	2.1	7.82	[32]
Cascaded FPIs	2.97	10.45	[37]
MI	1.36	10.37	[21]
Dual FPIs	1.59	1.17	[38]
Hybrid FPIs	5.2	13	[23]
MZI	-1.4	9.8	[39]
Intrinsic FPI	6.9	0.95	[40]
MI+FPI	6.8	11.6	Our Work

length of FPI and MI. K_T and $K\varepsilon$ are the sensitivities for temperature and strain, respectively. By putting the sensitivity values in the matrix,

$$\begin{bmatrix} \Delta \lambda_{FP} \\ \Delta \lambda_{MI} \end{bmatrix} = \begin{bmatrix} 0.0116 & 0.0067 \\ 0.0014 & 0.0011 \end{bmatrix} \begin{bmatrix} \Delta \varepsilon \\ \Delta T \end{bmatrix} \quad (15)$$

By computing the inverse of the above matrix from Eqs (15), the coefficient matrix of the hybrid interferometer for simul-taneous measurement can be calculated as

$$\begin{bmatrix} \Delta \varepsilon \\ \Delta T \end{bmatrix} = \begin{bmatrix} 0.0879 & 0.0144 \\ 0.0184 & 0.1523 \end{bmatrix} \begin{bmatrix} \Delta \lambda_{FP} \\ \Delta \lambda_{MI} \end{bmatrix} \quad (16)$$

The sensitivity matrix states that the proposed hybrid sensor can measure the wavelength shift due to applied temperature and strain, simultaneously.

We developed several samples of the proposed sensor during the experiments, which proved the stability and reproducibil-ity of the hybrid structure. The preparation of the hybrid interferometer only involves simple steps of cleaving, fusion splicing, and tapering, which also guarantees that fabrication procedure of the sensor is not complicated and the sensor can be reproduced easily. As for the performance of the hybrid sensor is concerned, the proposed hybrid sensor performs better than many sensors already reported in the literature, as shown in Table III.

IV. CONCLUSION

In this paper, a hybrid interferometer is proposed and investigated experimentally for measuring temperature and strain, simultaneously. This hybrid design is composed of Fabry-Perot interferometer (FPI) and Michelson Interferom-eter (MI) cascaded with each other. It is developed by fusion splicing, a single mode fiber (SMF), a multimode fiber (MMF), a dual side hole fiber (DSHF), a hollow core fiber (HCF) and a tapered-SMF. The tapered SMF was inserted into the HCF to form a reflection mirror for the FPI. The maximum temperature and strain sensitivity of the hybrid interferometer achieved through experiments is 11.6 pm/°C and 6.8 pm/$\mu\varepsilon$, respectively. The different sensitivities of FPI and MI to temperature and strain enable us to achieve simultaneous measurement. The proposed hybrid interferometer sensor has many attractive features for instance, novel design, low cost, easy fabrication, compact size, and good sensitivity. Therefore,

the proposed hybrid sensor could be widely deployed in plenty of applications, for instance, structural health monitoring, civil engineering, food manufacturing, chemical and medical fields.

REFERENCES

[1] D. Tosi, E. Schena, C. Molardi, and S. Korganbayev, "Fiber optic sensors for sub-centimeter spatially resolved measurements: Review and biomedical applications," *Opt. Fiber Technol.*, vol. 43, pp. 6–19, Jul. 2018.

[2] N. Bidin, N. H. Zainuddin, S. Islam, M. Abdullah, F. M. Marsin, and M. Yasin, "Sugar detection in adulterated honey via fiber optic displacement sensor for food industrial applications," *IEEE Sensors J.*, vol. 16, no. 2, pp. 299–305, Jan. 2016.

[3] K. Nazeri *et al.*, "Hollow-core photonic crystal fiber Mach–Zehnder interferometer for gas sensing," *Sensors*, vol. 20, no. 10, p. 2807, May 2020.

[4] A. Leal-Junior, L. Avellar, A. Frizera, and C. Marques, "Smart textiles for multimodal wearable sensing using highly stretchable multiplexed optical fiber system," *Sci. Rep.*, vol. 10, no. 1, pp. 1–12, Aug. 2020.

[5] J. M. López-Higuera, L. Rodriguez-Cobo, A. Q. Incera, and A. Cobo, "Fiber optic sensors in structural health monitoring," *J. Lightw. Technol.*, vol. 29, no. 4, pp. 587–608, Feb. 15, 2011.

[6] R. Min, Z. Liu, L. Pereira, C. Yang, Q. Sui, and C. Marques, "Optical fiber sensing for marine environment and marine structural health monitoring: A review," *Opt. Laser Technol.*, vol. 140, Aug. 2021, Art. no. 107082.

[7] S. Minakuchi and N. Takeda, "Recent advancement in optical fiber sensing for aerospace composite structures," *Photon. Sensors*, vol. 3, no. 4, pp. 345–354, 2013.

[8] Z. Zheng, Y. Yu, X. Zhang, Q. Guo, and H. Sun, "Femtosecond laser inscribed small-period long-period fiber gratings with dual-parameter sensing," *IEEE Sensors J.*, vol. 18, no. 3, pp. 1100–1103, Feb. 2018.

[9] W. Zhang, J. Hao, X. Lou, M. Dong, and L. Zhu, "All-fiber dual-parameter sensor based on cascaded long period fiber grating pair fabricated by femtosecond laser and CO_2 laser," *Fiber Integr. Opt.*, vol. 37, no. 2, pp. 66–78, Mar. 2018.

[10] W. Zhang, J. Hao, M. Dong, X. Lou, and L. Zhu, "A dual-parameter sensor for strain and temperature measurement featuring cascaded LPFG-FP structure," *Optik*, vol. 171, pp. 632–641, Oct. 2018.

[11] C. A. F. Marques, L. Bilro, L. Kahn, R. A. Oliveira, D. J. Webb, and R. N. Nogueira, "Acousto-optic effect in microstructured polymer fiber Bragg gratings: Simulation and experimental overview," *J. Lightw. Technol.*, vol. 31, no. 10, pp. 1551–1558, May 15, 2013.

[12] H. Zeng *et al.*, "Combining two types of gratings for simultaneous strain and temperature measurement," *IEEE Photon. Technol. Lett.*, vol. 28, no. 4, pp. 477–480, Feb. 15, 2016.

[13] X. Gao *et al.*, "A dual-parameter fiber sensor based on few-mode fiber and fiber Bragg grating for strain and temperature sensing," *Opt. Commun.*, vol. 454, Jan. 2020, Art. no. 124441.

[14] Y. Jiang, C. Liu, W. Zhang, D. Mao, D. Yang, and J. Zhao, "Multi-parameter sensing using a fiber Bragg grating inscribed in dual-mode fiber," *IEEE Photon. Technol. Lett.*, vol. 29, no. 19, pp. 1607–1610, Oct. 1, 2017.

[15] A. G. Leal-Junior, C. A. R. Díaz, A. Frizera, C. Marques, M. R. N. Ribeiro, and M. J. Pontes, "Simultaneous measurement of pressure and temperature with a single FBG embedded in a polymer diaphragm," *Opt. Laser Technol.*, vol. 112, pp. 77–84, Apr. 2019.

[16] X. Yu, X. Chen, D. Bu, J. Zhang, and S. Liu, "In-fiber modal interferometer for simultaneous measurement of refractive index and temperature," *IEEE Photon. Technol. Lett.*, vol. 28, no. 2, pp. 189–192, Jan. 15, 2016.

[17] B. Dong, Y. Peng, Y. Wang, and C. Yu, "Mode division multiplexing in a fiber modal interferometer for dual-parameters measurement," *IEEE Photon. Technol. Lett.*, vol. 28, no. 2, pp. 143–146, Jan. 15, 2016.

[18] T. Geng *et al.*, "Modal interferometer using three-core fiber for simultaneous measurement strain and temperature," *IEEE Photon. J.*, vol. 8, no. 4, pp. 1–8, Aug. 2016.

[19] J. Zhang *et al.*, "Simultaneous measurement of refractive index and temperature using a Michelson fiber interferometer with a Hi-Bi fiber probe," *IEEE Sensors J.*, vol. 13, no. 6, pp. 2061–2065, Jun. 2013.

[20] S. Zhang, L. Yin, Y. Zhao, A. Zhou, and L. Yuan, "Bending sensor with parallel fiber Michelson interferometers based on Vernier-like effect," *Opt. Laser Technol.*, vol. 120, Dec. 2019, Art. no. 105679.

[21] Y. Zhao *et al.*, "An integrated fiber Michelson interferometer based on twin-core and side-hole fibers for multiparameter sensing," *J. Lightw. Technol.*, vol. 36, no. 4, pp. 993–997, Feb. 15, 2018.

[22] F. Zhu, Y. Zhang, Y. Qu, H. Su, Li Zhao, and Y. Guo, "Fiber-optic hybrid structure sensor for simultaneous measurement of transverse load and temperature," *Optik*, vol. 208, Apr. 2020, Art. no. 164078.

[23] A. Zhou *et al.*, "Hybrid structured fiber-optic Fabry–Pérot interferometer for simultaneous measurement of strain and temperature," *Opt. Lett.*, vol. 39, no. 18, pp. 5267–5270, Sep. 2014.

[24] W. Peng, X. Zhang, Z. Gong, and Y. Liu, "Miniature fiber-optic strain sensor based on a hybrid interferometric structure," *IEEE Photon. Technol. Lett.*, vol. 25, no. 24, pp. 2385–2388, Dec. 15, 2013.

[25] Z. Li, Y.-X. Zhang, W.-G. Zhang, L.-X. Kong, and T.-Y. Yan, "Micro-cap on 2-core-fiber facet hybrid interferometer for dual-parameter sensing," *J. Lightw. Technol.*, vol. 37, no. 24, pp. 6114–6120, Dec. 15, 2019.

[26] X. Ni, M. Wang, D. Guo, H. Hao, and J. Zhu, "A hybrid Mach–Zehnder interferometer for refractive index and temperature measurement," *IEEE Photon. Technol. Lett.*, vol. 28, no. 17, pp. 1850–1853, Sep. 1, 2016.

[27] X. Gao *et al.*, "Simultaneous measurement of refractive index, strain, and temperature based on a Mach–Zehnder interferometer with hybrid structure optical fiber," *Appl. Opt.*, vol. 58, no. 30, pp. 8187–8193, Oct. 2019.

[28] B. Huang *et al.*, "In-fiber Mach–Zehnder interferometer exploiting a micro-cavity for strain and temperature simultaneous measurement," *IEEE Sensors J.*, vol. 19, no. 14, pp. 5632–5638, Jul. 2019.

[29] M. Najari, A. M. Javan, and N. Amiri, "Hybrid all-fiber sensor for simultaneous strain and temperature measurements based on Mach–Zehnder interferometer," *Optik Int. J. Light Electron Opt.*, vol. 126, no. 19, pp. 2022–2025, Oct. 2015.

[30] C. Zhu, R. E. Gerald, and J. Huang, "A dual-parameter internally calibrated Fabry–Pérot microcavity sensor," *IEEE Sensors J.*, vol. 20, no. 5, pp. 2511–2517, Mar. 2020.

[31] H. Sun *et al.*, "A hybrid fiber interferometer for simultaneous refractive index and temperature measurements based on Fabry–Pérot/Michelson interference," *IEEE Sensors J.*, vol. 13, no. 5, pp. 2039–2044, May 2013.

[32] X. Zhang, W. Peng, Li-Y. Shao, W. Pan, and L. Yan, "Strain and temperature discrimination by using temperature-independent FPI and FBG," *Sens. Actuators A, Phys.*, vol. 272, pp. 134–138, Apr. 2018.

[33] Y. Wu, Y. Zhang, J. Wu, and P. Yuan, "Fiber-optic hybrid-structured Fabry–Pérot interferometer based on large lateral offset splicing for simultaneous measurement of strain and temperature," *J. Lightw. Technol.*, vol. 35, no. 19, pp. 4311–4315, Oct. 1, 2017.

[34] O. Frazão, S. F. Silva, J. Viegas, J. M. Baptista, J. L. Santos, and P. Roy, "A hybrid Fabry–Pérot/Michelson interferometer sensor using a dual asymmetric core microstructured fiber," *Meas. Sci. Technol.*, vol. 21, no. 2, Feb. 2010, Art. no. 025205.

[35] T. Huang, S. Fu, C. Ke, P. P. Shum, and D. Liu, "Characterization of fiber Bragg grating inscribed in few-mode silica-germanate fiber," *IEEE Photon. Technol. Lett.*, vol. 26, no. 19, pp. 1908–1911, Oct. 1, 2014.

[36] W. Jin *et al.*, "Strain and temperature characteristics of the LP_{11} mode based on a few-mode fiber Bragg grating and core-offset splicing," *Laser Phys.*, vol. 28, no. 2, 2018, Art. no. 025103.

[37] J. Tian, Y. Jiao, S. Ji, X. Dong, and Y. Yao, "Cascaded-cavity Fabry–Pérot interferometer for simultaneous measurement of temperature and strain with cross-sensitivity compensation," *Opt. Commun.*, vol. 412, pp. 121–126, Apr. 2018.

[38] Y. Ouyang *et al.*, "An in-fiber dual air-cavity Fabry–Pérot interferometer for simultaneous measurement of strain and directional bend," *IEEE Sensors J.*, vol. 17, no. 11, pp. 3362–3366, Jun. 2017.

[39] T. Y. Hu and D. N. Wang, "Optical fiber in-line Mach–Zehnder interferometer based on dual internal mirrors formed by a hollow sphere pair," *Opt. Lett.*, vol. 38, no. 16, pp. 3036–3039, Aug. 2013.

[40] P. A. R. Tafulo, P. A. S. Jorge, J. L. Santos, F. M. Araujo, and O. Frazao, "Intrinsic Fabry–Pérot cavity sensor based on etched multimode graded index fiber for strain and temperature measurement," *IEEE Sensors J.*, vol. 12, no. 1, pp. 8–12, Jan. 2012.

Lashari Ghulam Abbas received the bachelor's degree in telecommunication engineering and the master's degree in computer communication from Sukkur IBA University, Sukkur, Pakistan, in 2010 and 2014, respectively. He is currently pursuing the Ph.D. degree with the National Engineering Laboratory for Fiber Optic Sensing Technology, Wuhan University of Technology, Wuhan, China. His current research interest is in the development of fiber optic interferometric sensors.

Zhou Ai received the B.S. degree in electronic science and technology, the M.Eng. degree in optical engineering and the Ph.D. degree in photonics from Harbin Engineering University, China, in 2003, 2005, and 2009, respectively. From 2004 to 2014, she was with the College of Science, Harbin Engineering University. In 2015, she joined the National Engineering Laboratory for Fiber Optic Sensing Technology, Wuhan University of Technology, Wuhan, China. Her research interests include fiber-optic sensing and fiber gratings.

Farhan Mumtaz was born in Islamabad, Pakistan, in 1985. He received the M.Phil. degree in electronics from Quaid-i-Azam University, Islamabad, in 2018, and the Ph.D. degree in information and communication engineering from the Wuhan University of Technology, Wuhan, China, in 2021. He has been worked with Huawei Technologies, Pakistan on several key positions as a Senior Manager Service Solution Sales, a Project Manager, and a Planning Control Manager. His current area of research interests include the design and development of optical sensors, optical waveguides, Femto-Laser micromachining, computational electromagnetics, and electromagnetic compatibility.

Atta Muhammad received the B.E. degree in telecommunication engineering and the M.S. degree in computer science from Sukkur IBA University, Sukkur, Pakistan, in 2010 and 2015, respectively. He is currently working as an Assistant Professor with the Telecommunication Engineering Department, Quaid-e-Awam University of Engineering, Science and Technology, Nawabshah, Pakistan. His current research interest is in the development of new fiber optic sensors.

Yutang Dai was born in Hubei, China, in 1965. He received the master's degree from the Huazhong University of Science and Technology, China, in 1989, and the Ph.D. degree from the Nippon Institute of Technology, Japan, in 2001. Then, he researched the ultra-precision micromachining technique of optoelectronic materials for four years in the Institute of Physical and Chemical Research (RIKEN), Japan. Presently, he is serving as a Professor with the National Engineering Laboratory of Fiber Optical Sensing Technology, Wuhan University of Technology, China. His current interests include femtosecond laser micromachining of optoelectronic materials and the development of new-type fiber optical sensors.

Rashda Parveen received the M.Phil. degree in electronics from Quaid-i-Azam University, Islamabad, Pakistan, in 2018, where she is currently pursuing the Ph.D. degree in electronics. She worked on state engineering in cavity opto-mechanics during her graduate research. Her recent research interests include wireless sensors networks and interaction of electromagnetic waves with anisotropic and complex media.